An Approach to Shape Parameterization Using Laboratory Hypervelocity Impact Experiments

John H. Seago[1], Heather Cowardin[2], Phillip Anz-Meador[3], Alyssa Manis[4], Joshua Miller[5], Eric Christiansen[6]

[(1)]ERC—Jacobs JETS II Contract, NASA Johnson Space Center,
MC XI5-9E, 2101 NASA Pkwy, Houston, TX 77058, USA, john.h.seago@nasa.gov
[(2)]NASA Orbital Debris Program Office, NASA Johnson Space Center,
MC XI5-9E,2101 NASA Pkwy, Houston, TX, 77058, USA, heather.cowardin@nasa.gov
[(3)]Jacobs, NASA Johnson Space Center,
MC XI5-9E, 2101 NASA Pkwy, Houston, TX 77058, USA, phillip.d.anz-meador@nasa.gov
[(4)]NASA Orbital Debris Program Office, NASA Johnson Space Center,
MC XI5-9E,2101 NASA Pkwy, Houston, TX, 77058, USA, alyssa.p.manis@nasa.gov
[(5)]University of Texas at El Paso, El Paso, TX 79968, USA, joshua.e.miller@nasa.gov
[(6)]Hypervelocity Impact Technology, NASA Johnson Space Center,
MC XI5-9E, 2101 NASA Pkwy, Houston, TX, 77058, USA, eric.l.christiansen@nasa.gov

Abstract

NASA's Orbital Debris Program Office relies on laboratory-based impact tests to supplement the measurement data of on-orbit events that define the orbital debris environment. These experiments deliver information that is essential to interpreting the radar and optical measurements of orbital fragmentation events into useful metrics, such as characteristic size, and to providing a better understanding of the distributions of fragment populations in terms of their masses, material constituents, fragment densities, cross-sectional areas, area-to-mass ratios, shapes, *etc*. The Satellite Orbital Debris Characterization Impact Test was a notable laboratory impact experiment conducted in 1992 using a surplus U.S. Navy Transit navigation satellite of the 1960s. The data from this ground-based experiment were combined with on-orbit measurements to develop the NASA Standard Satellite Breakup Model (SSBM). To account for advancements in satellite design and construction since, a new impact test series – DebriSat – was conducted in 2014. This test utilized a high-fidelity mock-up spacecraft that better represents the materials and construction techniques used to design and manufacture modern spacecraft. Together, these tests offer valuable data to model an orbital debris environment composed of legacy and modern spacecraft.

This paper presents an overview of the two laboratory impact tests, comparing their fragment parameter distributions with each other and with relevant distributions from the NASA SSBM. The categorization and descriptions of fragment shapes are of significant interest for future work, yet there are marked differences in the definitions of shape categories, categorizations of constituent materials, and the measurement techniques employed to populate these two datasets. New rubrics simplify and equate the categorizations between datasets to aid comparative analyses and to facilitate the potential use of both datasets in tandem with future environmental debris models. A preferred approach to classifying shape across disparate datasets uses the characteristic-length dimensions, and a simplified shape classification based on physical, solid-body dimensions, to mathematically construct an encapsulating right-circular cylinder that represents the fragment. The ratio of cylinder length-to-diameter (*L*:*D*) then provides a single continuum value for shape that is strongly correlated with its designated shape and size. This metric can then be used to further assess the distribution of shape with populations of other fragment characteristics within these datasets. The shape parameterization using the *L*:*D* ratios of right-circular cylinders is discussed.

1 The SOCIT and DebriSat Impact Experiments

The Satellite Orbital Debris Characterization Impact Test (SOCIT) tests were a series of hypervelocity impact tests with test dates spanning from December 1991 to January 1992. The fourth test, SOCIT4, targeted a flight-ready Navy Transit satellite bus. Current breakup models like the NASA Standard Satellite Breakup Model (SSBM) [1] use the results from the SOCIT4 test, which analyzed about 59% of the spacecraft's total mass [2]. The SSBM modeled well the major on-orbit collision involving *Cosmos* 2251 – a legacy spacecraft – in 2009, but collisions in 2007 (*Fengyun*-1C) and 2009 (Iridium 33) were not as well represented due to the presence of high area-to-mass ratio materials. The DebriSat experiment builds upon the previous impact test data by utilizing more modern materials typical of low Earth orbit (LEO) satellites today to better represent evolving materials and technology that may fragment differently. DebriSat's post-impact processing targets the collection of satellite fragments greater than or equal to 2 mm [3].

Table 1. Fragment database parameters relevant to shape parameterizations [4].

	SOCIT4 / Transit	DebriSat
ID	Individual fragments, or groupings of similar fragments	Individual fragments
Material	5 categories + "other"	14 categories + "metal"
Shape	9 categories + "other"	5 categories + "flexible"
Orthogonal Projections	x, y, z (cm)	x, y, z (mm)
Characteristic Length	$L_C = (x + y + z)/3$	$L_C = (x + y + z)/3$
Cross-sectional area (average)	$L_C{}^2$	Weighted average of projected areas visible in 2-D images
Mass	Individual or group average (g)	Individual fragments (g)
Area-to Mass ratio	Ballistic coefficient (m^2/kg)	Cross-sectional area / mass
Volume	N/A	Calculated from convex-hull point cloud (mm^3)
Bulk Density	N/A	Mass/volume
Quantities (as of Jan. 2023)	4700+ fragments in 810 records (individuals or groups)	59272 fragments used* (205K+ individual fragments)

*Used fragments have recorded mass, dimensions, primary material, shape

2 The SOCIT and DebriSat Fragment Datasets

Special consideration has been given to a DebriSat dataset from January 2023, being assessed as part of an internal series of deeper analyses that might provide shape characterizations for future environmental debris models. For this work, DebriSat fragment records were chosen having non-zero database entries for mass, dimensions, volume, primary material, and shape assessment. Of the 205,000+ DebriSat fragments recorded as of January 2023, 28% met these criteria for the current analyses. Table 1 identifies parameters in the SOCIT and DebriSat impact fragment databases that are potentially relevant to shape characterizations, with recorded shape and orthogonal projections having the most significance. Orthogonal-projection measurements [5] have the following definitions (Fig. 1):

- x is the longest projected dimension across the fragment,
- y is the longest projected dimension orthogonal to x, and
- z is the longest projected dimension orthogonal to the x-y plane.

The average of these mutually perpendicular orthogonal projections produces a characteristic length, L_C, that is independent of the aspect angle or orientation of a remotely sensed object. Thus, L_C is a standard

metric of size for space-debris observations, especially with non-spherical, complex targets, where the returned radar cross section on an object can be correlated to L_C using the NASA Size Estimation Model. For DebriSat, these orthogonal projections are estimated from a point-cloud based on DebriSat fragment images (imaging also improves repeatability and verification).

For SOCIT, orthogonal projections were measured with calipers. Many smaller fragments were grouped together and massed, rather than characterized individually, due to the labor required to manually undertake measurements. The mass of each SOCIT grouping was divided by the number of fragments in that group to obtain an average mass representative of the individual group members. It is not clear how the three dimensions, shape designation, *etc*., of such grouping were averaged in SOCIT groups (DebriSat fragments are not grouped). For shape-assessment purposes, it is assumed that the SOCIT recorded group value for shape and dimension are representative of every member of that group.

Table 2. Proposed Equivalence of SOCIT and DebriSat Primary Material Categorizations with Simplified Density Categories (with Total Fragment Count Percentages)*

SOCIT4 Material	%	DebriSat Material	%	Category	Density
		○ CFRP	61%	**CFRP**	1.5 g/cm^3
• Fiberglass • Phenolic/Plastic	8% 68%	○ Epoxy ○ Polyimide film ○ Para-aramid synthetic fiber ○ Multi-Layer Insulation, MLI ○ Printed Circuit Board, PCB ○ Plastic ○ Silicon	6% 0.8% 0.4% 4% 1% 6% 0.8%	**Low Density** (LD)	< 2 g/cm^3
• Al • Other	22% 1%	○ Al ○ Glass ○ *Metal* ○ Solar Cell	5% 1% 2% 0.4%	**Medium-Low Density** (MD-lo)	2–4 g/cm^3
		○ Titanium	1%	**Medium-High Density** (MD-hi)	4–6 g/cm^3
• Copper • Steel	0.3% 0.7%	○ Copper ○ Steel)	9% 2%	**High Density** (HD)	> 6 g/cm^3
	100%		100%		

*DebriSat database contents as of January 27, 2023.

The varied material types for each laboratory experiment are shown in Table 2 with percentages of total fragment counts and grouped by density categories for analysis. A fragment is considered low density if the primary material density is below 2 g/cm^3 – excepting carbon-fiber reinforced polymer (CFRP), which is separated because of its unique predominance in the DebriSat fragment-count distribution. The remaining three categories are assigned according to primary material density: medium-low (2-4 g/cm^3), medium-high (4-6 g/cm^3), and high density (above 6 g/cm^3), with the understanding that assessed fragment densities based on primary material may not be homogenous. The metal category is a placeholder for metallic fragments that still require further verification to classify the metal type (the category is presumed here to have the density of aluminum).

SOCIT fragments were classified into 10 shape categories; DebriSat shape categories were reduced to 5 primary shapes and a generic flexible category after collaborations involving the NASA Orbital Debris Program Office and NASA's Hypervelocity Impact Technology (HVIT) team. To aid comparative analyses for this study, and to facilitate future environmental debris models, these categorizations were

simplified into three shapes: rods (having one relatively large dimension), plates (having one relatively small dimension), and nuggets (having similar dimensions), with two sub-categories for rods and plates: bent or unbent (see Table 3).

Comparing the total fragment count percentages of both impact tests in Table 3, nugget-like shapes dominate the SOCIT fragment counts, whereas for DebriSat it is flat plates and straight rods – this is due to the fragmentation behavior of CFRP dominant to DebriSat but absent from SOCIT [6]. DebriSat's flexible category reflects non-rigid items with variable or unreliably captured shapes due to flexure, typified by fabrics (*e.g.*, MLI); it was classified as bent plates for this work.

Table 3. Suggested Equivalence of SOCIT and DebriSat Shape Categorizations with Simplified Shape Categories (Total Fragment Count Percentages)

SOCIT4 / Transit		%	DebriSat		%	Simplified
• Flat Plate • Flake	(1%) (13%)	14%	○ Flat Plate	(36%)	36%	Plate
• Curled Plate	(1%)	1%	○ Flexible ○ Bent Plate	(1%) (2%)	3%	*Plate (Bent)*
• Box • Sphere • Box & Plate • Nugget • Other	(0.3%) (<0.1%) (<0.1%) (59%) (23%)	83%	○ Parallelepiped/nugget/spheroid	(19%)	19%	Nugget
			○ Bent needle/rod/cylinder	(11%)	11%	*Rod (Bent)*
• Rod • Cylinder	(2%) (0.3%)	2%	○ Straight needle/rod/cylinder	(31%)	31%	Rod
	(100%)	100%		(100%)	100%	

Table 4. Total Fragment Count Percentages by Simplified Shape Category

	Plates	*Plates (Bent)*	Nuggets	*Rods (Bent)*	Rods	Total
SOCIT	14%	1%	83%	2%	2%	100%
DebriSat (without CFRP)	**15%**	**7%**	**41%**	**28%**	**10%**	100%
DebriSat (with CFRP)	36%	3%	19%	11%	31%	100%

The percentage of total fragment counts by simplified shape for both tests are shown in Table 4, including DebriSat without CFRP. Because of its prominence in the DebriSat database, the omission of the CFRP changes the relative percentages of the DebriSat sample. Since CFRP flakes and splinters into plate-like and rod-like pieces primarily, if CFRP samples are omitted, then the DebriSat sample trends to nugget shapes. Without CFRP, most DebriSat rods are bent, since thin-wire segments comprising most of the non-CFRP rod-like fragments easily bend.

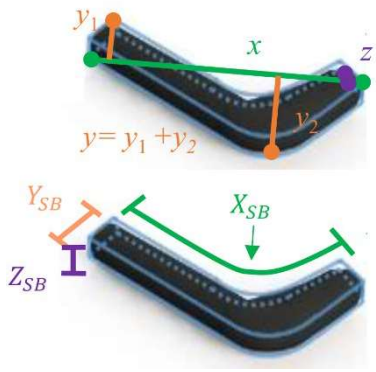

Fig. 1. Orthogonal-projections $x \geq y \geq z$ and solid-body dimensions $X_{SB} \geq Y_{SB} \geq Z_{SB}$ of a bent rod.

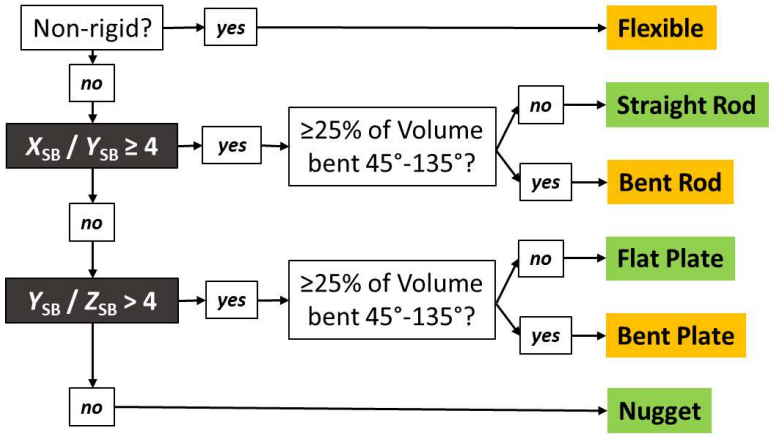

Fig. 2. Decision logic for characterizing DebriSat shapes based on solid-body dimensions $X_{SB} \geq Y_{SB} \geq Z_{SB}$ [8].

3 Shape Approximation via Right Circular Cylinders

The risks from non-spherical debris within the orbital debris environment are being actively studied by NASA's HVIT team using the outcomes of hypervelocity impact tests, coupled with hydrodynamic computer simulations. Hydrodynamic simulations extend the results from laboratory impact tests and better assess the damage on specific shields in a specified environment by accounting for the substantial number of parameters needed to analyze the damage from non-spherical projectiles [7]. NASA hypervelocity testing and simulations with non-spherical projectiles have used right-circular cylinders (RCCs), a general shape that can be more practically manufactured and launched than the original SOCIT and DebriSat shape categories from Table 3. The RCC shape can be characterized by a single shape parameter: the ratio of its length-to-diameter (L:D). Only two or three distinct shape proportions are required for mathematical estimation: rods and plates, with nuggets representing their transition.

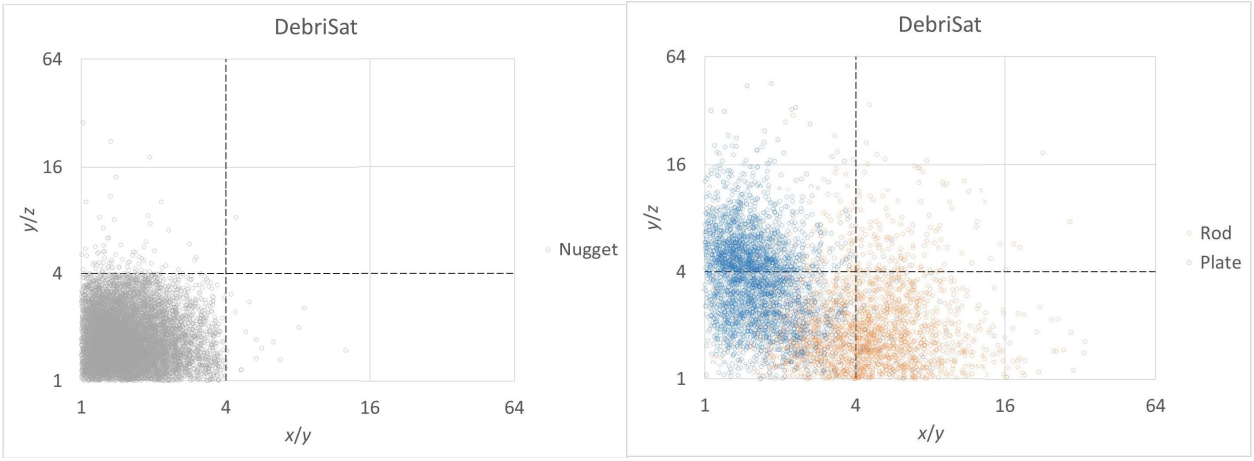

Fig. 3. Ratios of orthogonal-projection $x \geq y \geq z$ dimensions for unbent "nugget-like" (left) and "non-nugget-like" DebriSat fragments (right).

The SOCIT fragment processing demonstrated a need for more automated and objective assessments of shape and size. For DebriSat, a shape rubric was implemented to aid fragment shape categorization [6],

based on solid-body dimensions $X_{SB} \geq Y_{SB} \geq Z_{SB}$. These dimensions would maximize the fragment's inertia if the object were unbent and are assessed by visual inspection. Maximum-inertia values (X_{SB}, Y_{SB}, Z_{SB}) can be much different than the orthogonal-projection dimensions x, y, z recorded in the database, and shape assessments for bent or flexible objects require estimation by an inspector (Fig. 1). The logic of the decision tree to characterize DebriSat shapes is shown in Fig. 2. The assignment of rods is prioritized, which is based on a fragment's relative length and not thickness.

Because the original solid-body dimensions are unavailable, the orthogonal projections $x \geq y \geq z$ were used as proxies for $X_{SB} \geq Y_{SB} \geq Z_{SB}$ in scatterplot form to assess their potential for assessing shape. The scatterplot of Fig. 3 is the result for DebriSat; the behavior is similar for SOCIT data except that most rod-like objects reside on the $y/z = 1$ axis ($y = z$). If the DebriSat shape rubric (Fig. 2) is used as a benchmark for defining shapes, Fig. 3 suggests that orthogonal-projection dimensions seem quite consistent with the solid-body dimensions of nugget shapes (94% agreement for SOCIT, 99% for DebriSat), but less consistent with the solid-body dimensions of plates (43% agreement for SOCIT, 76% for DebriSat) or rods (69% agreement for SOCIT, 67% for DebriSat). For nuggets, orthogonal-projection dimensions will better approximate solid-body axes when the fragment shape has no sharp corners or protrusions (*e.g.*, $x \geq y \geq z$ are equivalent to $X_{SB} \geq Y_{SB} \geq Z_{SB}$ for ellipsoidal shapes, but not for cylinders or cuboids).

Most fragment bending is thought to occur during impact with the foam catch system. The orthogonal-projections of a deformed plate or rod will imply a shape that is far more nugget-like than its original pre-impact shape, so that impact bending renders estimates of shape from the recorded x, y, z unreliable. Bent fragments are consequently omitted from Fig. 3 and other L:D estimates and L:D distributions in this work. Although it appears reasonable to use $x \geq y \geq z$ to estimate a shape parameter for the nugget class, there is a need to better approximate the solid-body dimensions of plates and rods for the estimation of L:D.

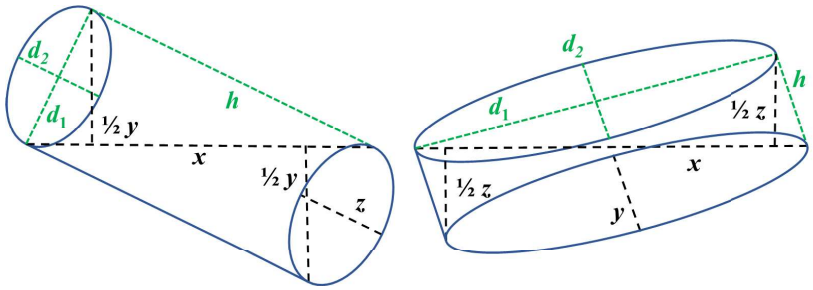

Fig. 4. Solid-body axes (h, d_1, d_2) and orthogonal-projection ($x \geq y \geq z$) dimensions for rod-like (left) and plate-like (right) elliptical cylinders.

4 *L*:*D*-Ratio Estimation Based on the Orthogonal-Projection Dimensions of a Cylinder

Fig. 4 illustrates a relationship between the orthogonal projections and the solid-body axes of rod-like and plate-like elliptical cylinders, where h is the height of the cylinder, and d_1 and d_2 are the major and minor diameters of the elliptical flats, respectively, and $D = (d_1\, d_2)^{½}$. Thus, when $h > D$, an RCC is rod-like and when $h < D$, an RCC is plate-like. For a rod where $x > y > z$, the values of h and d_1 reside in the same plane as x and y, such that an estimate of h^2 can be developed from plane geometry (Table 5). A solution applicable to plate-like cylinders can also be derived, where y and z are swapped per Fig. 4. If (h, d_1, d_2) are used as proxies for the solid-body dimensions when employing the DebriSat shape-decision logic

(Fig. 2), the correlation with the database-assigned fragment shapes generally improves for plates and rods, relative to the use of orthogonal projections as proxies, per Table 6.

Table 5. Relationships between Orthogonal Projection Dimensions ($x \geq y \geq z$) and Cylinder Solid-Body Axes (h, d_1, d_2)

	"Rod-like"	"Plate-like"
$h^2 =$	$\frac{1}{2}\left(1+\sqrt{1-\left(\frac{y}{x}\right)^2}\right)x^2$	$\frac{1}{2}\left(1-\sqrt{1-\left(\frac{z}{x}\right)^2}\right)x^2$
$d_1 =$	$\frac{yx}{2h}$	$\frac{zx}{2h}$
$d_2 =$	z	y

Table 6. Percentage of Fragments Whose Assigned Shape **Matches** the DebriSat Decision Tree Logic When Approximating ($X_{SB} \geq Y_{SB} \geq Z_{SB}$) as Either ($x \geq y \geq z$) or ($h$, d_1, d_2)

	Plates		*Rods*	
	($x \geq y \geq z$)	(h, d_1, d_2)	($x \geq y \geq z$)	(h, d_1, d_2)
SOCIT	43%	75%	*69%*	*69%*
DebriSat	76%	92%	67%	88%
DebriSat (w/o CFRP)	37%	75%	26%	67%
DebriSat (w/o CFRP, unbent only)	46%	84%	57%	83%
DebriSat (w/o CFRP, bent only)	16%	56%	16%	62%

Table 7. RCC Shape Parameterization from an Ellipsoidal Volume.

RCC Dimensions	Flat Plate	Nugget/ Spheroid	Straight Rod
$L:D$	$\frac{4\,V}{\pi}(d_1\,d_2)^{-\frac{3}{2}}$	$\sqrt{\frac{\pi\,y^3}{4\,V}}$	$\sqrt{\frac{\pi\,h^3}{4\,V}}$

Given a transformation from (x, y, z) to (h, d_1, d_2) from Table 5, an L:D ratio can be estimated geometrically from $L = h$ and $D = (d_1\,d_2)^{½}$. This estimator assumes that the irregular fragment is dimensionally a cylinder with a geometric volume:

$$V = \pi\,h\left(\frac{D}{2}\right)^2 \quad , \; D = \sqrt{d_1\,d_2}\,. \tag{1}$$

This volume can be substituted into the L:D ratio $h\,(d_1\,d_2)^{-½}$ through a change of variable(s).

Table 7 presents estimators of L:D ratio for the three (unbent) simplified shape categories of Table 4 in terms of V from Eq. (1). Cylinders that are nugget-like are already well represented by spherical impactors used in prior models, testing, and simulation, so a useful L:D definition for nuggets need only sensibly assign L:D values between those of plates and rods using orthogonal-projections most appropriate for nuggets (see Fig. 3). For nuggets, the central orthogonal-projection dimension, y, is assumed to be a representative length for a "stubby rod" L:D estimator, which appears to provide a

slightly improved distributional separation (minimal overlap) of nugget *L*:*D* values from those of rods and plates compared to a "thick plate" representation. For example, a stubby rod provided ~99% of *L*:*D* estimates for plates and rods *outside* the range of 1:2 < *L*:*D* < 2:1 ($10^{\pm 0.3}$), whereas over 90% of the nugget samples fell *inside* 1:2 < *L*:*D* < 2:1 (see Fig. 5).

Table 8. Advantages and Disadvantages of Various Fragment Volume Estimators

Volume Type	Expression	Advantages	Disadvantages
Geometric	$\frac{1}{4}\,\pi\, d_1\, d_2\, h$	• Definable for all usable fragments from $x \geq y \geq z$ only	• Assumes a cylindrically shaped fragment was measured
Bulk	"Measured"	• Based on observed fragment dimensions (actual shape) • Distributionally well-behaved	• No bulk volumes recorded for SOCIT
Mass	m / ρ	• Definable for all usable fragments • Explicit function of mass • Conservative risk assessments	• Fragment densities approximate, based only on primary material • Materials not always accurate • Shape distributions spread out

Fragment volume *V* can be estimated in multiple ways, as described in Table 8. A geometric volume assumes a cylindrical shape, and Eq. (1) is employed. A bulk volume is a recorded measurement (*e.g.*, a 3-D surface hull from shape carving algorithms or point clouds [9], or a 2-D perimeter contour multiplied by a fragment thickness). The mass-based volume is the recorded mass (*m*) divided by the assumed material density ρ, independent of dimensional information. All volume estimation methods provide equivalent outcomes for a laboratory projectile, which is a true cylinder with consistent geometry, mass, and known material density, but each volume estimator provides a different result for an irregular (non-cylindrical) fragment.

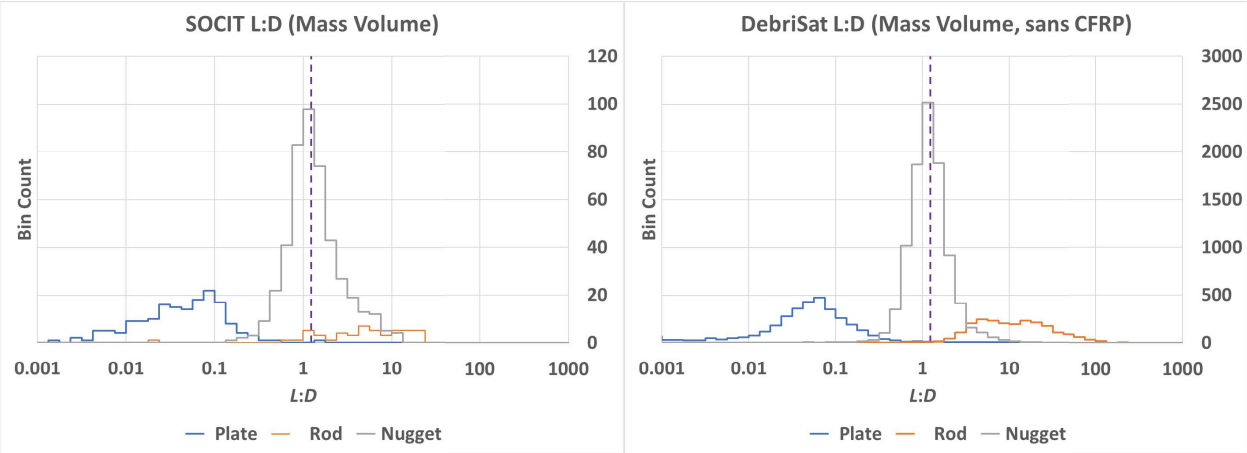

Fig. 5. Distributions of estimated *L*:*D* ratio for simplified shapes based on $V = m/\rho$.
Bent shapes omitted. CFRP omitted from DebriSat, and SOCIT counts based on groups.
Dashed vertical indicates stubby rod with spherical volume.

Fig. 5 illustrates that the *L*:*D* estimates for each shape category cluster into regions that are roughly log normal. This clustering behavior exists regardless of the volume estimator employed and is mostly a

consequence of having three shape-dependent estimators that drive *L*:*D* estimates to a particular *L*:*D* region ($L{:}D_{plate} < 1$, $L{:}D_{rod} > 1$, and $L{:}D_{nugget} \approx 1$). The effect can be illustrated by considering a hypothetical cylinder at the intersection of $X_{SB}/Y_{SB} = Y_{SB}/Z_{SB} = 4$ in Fig. 3, and thus is potentially assignable during inspection as either a plate, rod, or nugget. The geometric *L*:*D* estimates will differ significantly depending on the shape assigned, given the static cylindrical proportions of [4 : 1 : ¼]: $L{:}D_{plate}$ = 1:8 (< 1), $L{:}D_{rod}$ = 8:1 (> 1), and $L{:}D_{nugget} \approx$ 27:10 (~1). Therefore, a fragment's designated shape predestines the magnitude of its *L*:*D* ratio, and the fragment's relative dimensions add precision to its *L*:*D* estimate. SOCIT distribution counts are noticeably less than DebriSat because each grouping of SOCIT samples – mostly nuggets – count as just one representative *L*:*D* ratio. The broken vertical line indicates *L*:*D* ≈1.225, the value for a sphere of diameter *y* modeled as a stubby rod (per Table 7).

Table 8 assesses the pros and cons of each approach; notably, a bulk volume is *not* ordinarily available for SOCIT, and the cylindrical assumption of the geometric volume might be too unrealistic to employ with ballistic damage equations. Therefore, an investigation was conducted into how a geometrical volume assumption compares with the other two volume calculations. To illustrate the variation that can occur using different volume estimators, Table 9 provides estimates of the central tendency of each condensed shape (plates, nuggets, rods) for several sample sub-populations, using the volume estimators described in Table 8. A central *L*:*D* ratio, $L{:}D_{ave}$, for each condensed shape category can be estimated from histograms like Fig. 5, based on a weighted average of their bin counts:

$$L{:}D_{ave} = \frac{\sum_{i=1}^{nbins} n_i \cdot (L{:}D)_i}{\sum_{i=1}^{nbins} n_i} \qquad (2)$$

where n_i is the number of *L*:*D* estimates within the i^{th} bin centered on $L{:}D_i$. *L*:*D* estimates from weighted-averages – which are not necessarily the most frequent values (modes or histogram peaks) – are notional as they can vary depending upon the bin limits established for the shape categories, whether the results are weighted per group or per fragment (for SOCIT), and the volume estimator used. For Table 9, averages for plates were estimated from bins of $L{:}D_i < 10^{-1/2}$, rods from bins of $L{:}D_i > 10^{+1/2}$, and nuggets between $10^{\pm 1/2}$.

Table 9. Average L:D Estimates Using Different Volume Estimators Over Fragment Populations
Bent Shapes Omitted, and SOCIT Counts Weighted by Group (not per fragment).

		Mass-based, $V = m/\rho$			Bulk, *V* "observed"			Geometric, $V = ¼\ \pi\ h\ d_1\ d_2$		
		Plates	Nuggets	Rods	Plates	Nuggets	Rods	Plates	Nuggets	Rods
SOCIT	All	1:20	1:1	9:1	--	--	--	1:11	1:1	21:1
DebriSat	All	1:30	2:1	19:1	1:13	1:1	14:1	1:19	1:1	16:1
DebriSat	w/o CFRP	1:19	1:1	15:1	1:9	1:1	12:1	1:10	1:1	10:1
DebriSat	CFRP only	1:32	2:1	20:1	1:14	1:1	14:1	1:21	2:1	17:1
SOCIT	LD	1:20	1:1	7:1	--	--	--	1:14	1:1	10:1
DebriSat	LD	1:21	1:1	12:1	1:9	1:1	10:1	1:10	1:1	10:1
SOCIT	MDlo	1:20	2:1	8:1	--	--	--	1:9	1:1	21:1
DebriSat	MDlo	1:15	1:1	9:1	1:8	1:1	8:1	1:8	1:1	7:1
DebriSat	MDhi	1:17	1:1	7:1	1:10	1:1	7:1	1:12	1:1	7:1
SOCIT	HD	1:6	1:1	11:1	--	--	--	1:12	1:1	28:1
DebriSat	HD	1:33	2:1	23:1	1:13	1:1	15:1	1:10	1:1	11:1

Table 9 demonstrates that geometric and bulk estimate values are in closer agreement for many density regions than the mass-based approach, which can produce more exaggerated *L*:*D* estimates – especially for DebriSat – potentially unrealistic for hypervelocity experiments used for non-spherical projectile risk assessments. The CFRP results tend to be more varied; this is possibly due to the complex nature of the CFRP fragments that can produce plate-like objects with vertical dimensions. Provided the direct geometric volume requires the assumption all fragments are cylinders, the application of either geometric or bulk volumes to *L*:*D* estimation is a feasible methodology for modeling on-orbit shape distributions with empirical data from laboratory experiments.

5 Conclusions and Future Work

Modeling irregular fragment shapes as right-circular cylinders is advantageous because cylinders are a practical shape for laboratory hypervelocity-impact testing, and the RCC shape can be described with one parameter, the *L*:*D* ratio. The mass and mass distribution (density) of a fragment can be introduced into the *L*:*D* estimator via fragment volume by a change of variable(s). The DebriSat dataset offers a mass-based volume (mass-over-density) and a bulk volume estimated from fragment imaging, but volume estimates for SOCIT fragments are only mass-based. An investigation into the use of geometrical volumes, based only on orthogonal-projection dimensions, suggests the feasibility of using a cylindrical geometric volume for *L*:*D* ratio estimation when bulk volume is unavailable, such as with SOCIT; however, mass-based *L*:*D* is always available, and it may be more useful for ballistic modeling purposes. A geometric approach depends only on physical dimension, whereas a mass-based approach leverages other characteristics. Future work should consider *L*:*D* ratio estimation of significantly bent fragments.

6 References

1. Johnson, N.L., *et al*. “NASA’s New Breakup Model of EVOLVE 4.0,”Adv. Space Res., vol. 28, issue 9, pp. 1377-84, 2001.
2. D.M. Hogg, *et al.* “Final report on the SOCIT series of hypervelocity impact tests,” General Research Corporation, Santa Barbara, CA, USA, 1993, WL-TR-93-7025.
3. Liou, J.-C. *et al*. “Successful Hypervelocity Impacts of DebrisLV and DebriSat,” Orbital Debris Quarterly News, vol. 18, issue 3, pp. 3-6, 2014.
4. Ausay, E., *et al*., “A Comparison of the SOCIT and DebriSat Experiments,” European Conference on Space Debris, 2017.
5. Hill, N. “Measurement Techniques for Hypervelocity Impact Test Fragments,” 59th International Astronautical Congress, 29 September – 3 October 2008, Glasgow, Scotland, IAC-08-D6.3.10.
6. Cowardin, H., et al., “Updates on the DebriSat Hypervelocity Experiment and Characterization of Fragments in Support of Environmental Models,” International Journal of Impact Engineering, volume 180, October 2023, 104669.
7. Cowardin, H., *et al.* “Orbital Debris Shape Effect Investigations for Mitigating Risk,” 2023 AMOS Proceedings, 19-22 Sept 2023.
8. Murray, *et al*. “Analysis of the DebriSat Fragments and Comparison to the NASA Standard Satellite Breakup Model," Proceedings of the 1st International Orbital Debris Conference, Sugar Land, TX, USA, 2019.
9. Rivero, M., *et al*. "DebriSat Fragment Characterization System and Processing Status," 67th International Astronautical Congress, Guadalajara, Mexico, IAC-16.A6.2.8x35593.